Asian Journal of Chemistry; Vol. 37, No. 6 (2025), 1351-1357

ASIAN JOURNAL OF CHEMISTRY

https://doi.org/10.14233/ajchem.2025.33730

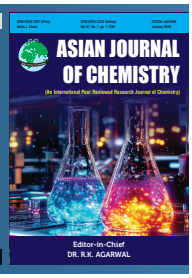

Solar Light Assisted Photocatalytic Degradation of Malachite Green Dye using $CoO/BiVO_4$ Nanocomposite: Kinetics and Mechanism Studies

PRAFULLA KUMAR PANDA, RASMIREKHA PATTANAIK, RISHABH KAMAL and SURESH KUMAR DASH*

Department of Chemistry, Faculty of Engineering and Technology, Siksha 'O' Anusandhan (Deemed to be University), Bhubaneswar-751030, India

*Corresponding author: E-mail: sureshdash@soa.ac.in

Received: 23 March 2025; *Accepted*: 30 April 2025; *Published online*: 27 May 2025; AJC-22008

Water pollution caused by dye discharge is a critical environmental concern, driving the exploration of efficient wastewater treatment methods using nanocomposites. This study presents the synthesis of a $CoO/BiVO_4$ nanocomposite, with CoO and $BiVO_4$ prepared through the co-precipitation process. The structural, morphological and optical properties of the synthesized catalyst were characterized using XRD, FESEM and UV-DRS analyses. The band gap energies, determined from Tauc's plot, were found to be 2.9 eV for pristine $BiVO_4$ and 2.5 eV for the $CoO/BiVO_4$ nanocomposite, indicating enhanced light absorption. The photocatalytic performance of the nanocomposite was evaluated by degrading malachite green dye under solar irradiation. Various parameters, including pH, catalyst dosage, dye concentration and irradiation time, were optimized to maximize degradation efficiency. The nanocomposite achieved 84% dye degradation at pH ~ 7 using 40 mg of catalyst on a 40 ppm dye solution within 80 min of solar exposure. Kinetic analysis revealed that the degradation followed a pseudo-first-order kinetic model. Moreover, the reusability of the catalyst was confirmed, showing stable performance even after five consecutive cycles. The findings highlight the potential of the $CoO/BiVO_4$ nanocomposite as a sustainable photocatalyst for effective dye degradation in wastewater treatment applications under solar light.

Keywords: $CoO/BiVO_4$, Malachite green dye, Photodegradation, Kinetics, Mechanism, Recyclability.

INTRODUCTION

Due to the increased industry and urbanization have exacerbated water pollution, especially in poor countries with limited access to effective water treatment facilities. Water sources are frequently polluted with microorganisms, organic pollutants and heavy metals, creating major public health risks and facilitating the spread of many illnesses. Further endangering human health and ecological balance is the increasing levels of organic micropollutants, including pesticides, antibiotics and polycyclic aromatic hydrocarbons, in natural aquatic systems and city wastewater [1-4]. Significant amounts of synthetic organic dyes are released into the effluents of industries including printing, dyeing and textiles. Non-biodegradable colours make up around 15% of these wastewater discharges or hundreds of tons per year, from the textile industry alone. As a result, eliminating these contaminants from wastewater is critical for environmental preservation [5]. First-generation catalysts, such as TiO_2, ZnO and Fe_3O_4, have been widely studied for their photocatalytic properties due to their high stability, non-toxicity and availability [6,7]. However, their effectiveness is limited by their large band gaps, low activity under visible light and rapid recombination of charge carriers [8]. These factors restrict their efficiency, especially under natural sunlight. The development of visible-light-driven (VLD) photocatalysts for wastewater treatment has been a major focus for researchers. Currently approximately 150 semiconductor materials available for environmental purification applications, including metal oxides, sulfides, carbides, halides, chalcogenides, oxyhalides and hydroxides [9].

$BiVO_4$ is an n-type semiconductor with outstanding chemical and photostability. Its adaptable optical and electrical characteristics, along with a band gap of about 2.4 eV, make it an appealing choice for effective solar energy harvesting [10,11]. $BiVO_4$ exists in three crystal structures: the tetragonal zircon phase (t-z), monoclinic scheelite phase (m-s) and tetragonal scheelite phase (t-s). Among these, the monoclinic scheelite

phase (m-s) $BiVO_4$ demonstrates superior photocatalytic performance under visible-light illumination. This is due to the lone pair distortion of the Bi 6*s* orbital in the $BiVO_4$ semiconductor, which enhances the overlap between the O 2*p* and Bi 6*s* orbitals in the valence band. This overlap facilitates the mobility of photogenerated charge carriers, leading to improved photocatalytic activity [12]. Thus, the bismuth-based metal oxides, including $BiVO_4$, Bi_2WO_3, Bi_2MoO_6, $Bi_4Ti_3O_{12}$, $BiFeO_3$, $Bi_2Fe_4O_9$, $Bi_5FeTi_3O_{15}$, BiOX (X = Cl, Br, I) and Bi_5O_7I, have become promising candidates among these materials due to their superior photocatalytic efficiency as a result of their improved charge transfer characteristics [13-17]. Moreover, the metal doping involves the development of heterojunction structures with other metal oxides, with vacancy manipulation and surface modification. In this work, $CoO/BiVO_4$ nanocomposites were synthesized *via* co-precipitation method followed by the structure, morphological, textural and optical properties of the as-prepared nanocomposites characterization. The photocatalytic experiments, employing direct sunlight have been performed on malachite green dye.

EXPERIMENTAL

Bismuth nitrate pentahydrate [$Bi(NO_3)_3{\cdot}5H_2O$], cobalt nitrate hexahydrate ($Co(NO_3)_2{\cdot}6H_2O$) and sodium hydroxide (NaOH) were sourced from Merck Ltd. India, with 99% purity. Conc. HNO_3 of highest purity was used. Deionized double-distilled (DI) water was utilized for solution preparation.

Synthesis of $BiVO_4$: $BiVO_4$ was synthesized through a co-precipitation method. First, $Bi(NO_3)_2{\cdot}5H_2O$ was dissolved in a 1 M HNO_3 solution in a 1:1 M ratio. Upon the formation of a reddish-yellow colour, 1 M NaOH solution was gradually added while stirring vigorously to raise the pH to 10. This resulted in a light yellow solution, which was washed multiple times with distilled water and then centrifuged. The filtrate was dried in an oven and calcined at 500 ºC in a muffle furnace for 3 h. Finally, the resulting yellow powder was finely ground and used for the application study.

Synthesis of $BiVO_4$/CoO: The synthesized $BiVO_4$ and CoO were mixed in different ratios with ethanol and distilled water and stirred for 2 h. To separate the agglomerated particles, the solution was centrifuged, washed with distilled water and then dried in an oven at 60 ºC for 8 h. The dried material was then calcined at 500 ºC, grind using a mortar and pestle and the $BiVO_4$/CoO composite was collected in a sample tube.

Characterization: The structural and morphological structure of $BiVO_4$ NPs was analyzed by X-ray diffraction (XRD) with Cu*K*α radiation (PW 1830, Philips, Japan) having 2θ range from 10º to 80º to acquire the diffraction patterns. The textural properties were analyzed by field emission scanning electron microscope (FE-SEM) by ZEISS SUPRA 55 and a transmission electron microscope (TEM) by JEOL/JEM2100. The elemental composition was investigated using EDS analysis. The UV-DRS spectra to investigate optical properties was done by a Perkin-Elmer Lamda365 spectrophotometer. To measure the specific surface area and pore size nitrogen adsorption/desorption instrument (Quantachrome Instruments v11.05) was used. Finally, to analyze the concentration of the malachite green dye solutions before and after the photodegradation tests, a UV-Vis spectrophometer (Systronics 2202) was used. A solar simulator equipped with a 300 W Xenon lamp (Newport, USA) was used as a light source.

Photocatalytic analysis: By examining the degradation of malachite green dye under solar light irradiation, the photocatalytic activity of the produced photocatalysts was evaluated. In 30 mL of 30 ppm malachite green dye solution, a predetermined quantity of photocatalyst was suspended. Before exposing the solution to visible light, it was magnetically agitated in the dark for 90 min to achieve adsorption-desorption balance. A Perkin-Elmer Lambda 35 UV-Vis spectrophotometer was used to measure the quantity of malachite green dye at λ_{max} = 616 nm during the photocatalytic degradation process. The percentage of photodegradation of malachite green dye was calculated using eqn. 1:

$$\text{Photodegradation (\%)} = \frac{C_o - C_t}{C_o} \times 100 \quad (1)$$

where C_o was the initial concentration of malachite green dye and C_t was the concentration of malachite green dye at time t.

RESULTS AND DISCUSSION

Structural studies: The structural and phase of the fabricated catalyst were studied using XRD analysis and the result is shown in Fig. 1. The XRD patterns of $BiVO_4$ shows a monoclinic scheelite structure with space group I2/b, a = 5.193, b = 5.089, c = 11.697 and γ = 90.387º. This matches the JCPDS

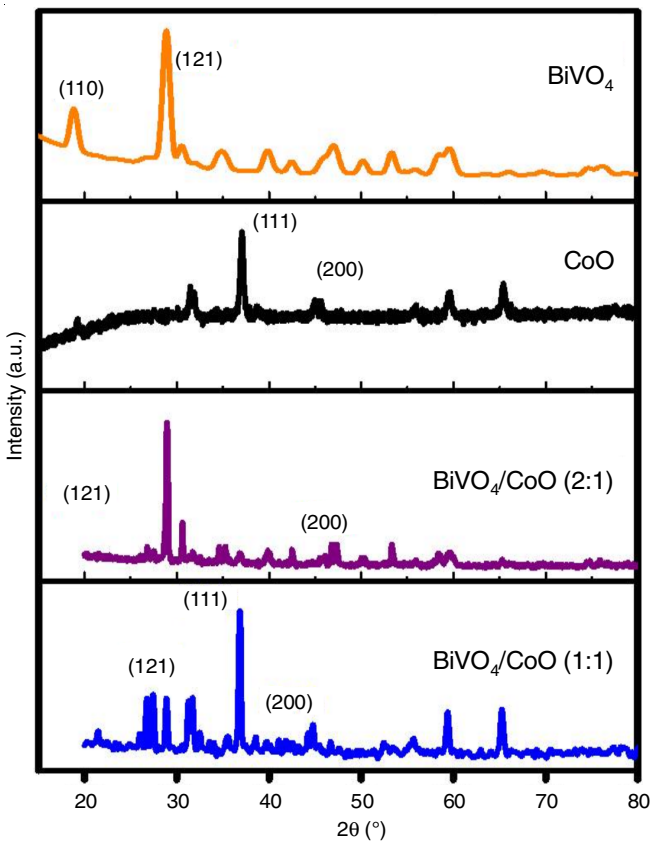

Fig. 1. XRD patterns of $BiVO_4$, CoO, $BiVO_4$/CoO (1:1), $BiVO_4$/CoO (2:1)

card No. 75-1866, indicating high material purity [18]. The found diffraction peaks at 2θ values of 18.6º, 28.7º, 34.5º, 35.2º, 39.5º, 45.7º, 46.9º, 49.9º, 53.2º, 55.7º, 58.2º and 59.0º, correspond to (001), (013), (004), (200), (020), (211), (015), (123), (204), (024). All of the peaks are related to the monoclinic phase of $BiVO_4$. Incase of CoO, the two crystal planes (111), (200), observed at approximately 2θ values of 36.87º, 42.39º and 49.9º correspond to the cubic phase of CoO. This is confirmed by the JCPDS file no. 75-0393, with a lattice constant of a = 0.4258 nm and a space group of $Fm\bar{3}m$ [19]. In case of heterojunction (1:1) of both the caharacteristic plane of $BiVO_4$ (121) and CoO (111) are present in well-defined manner but not incase of 2:1 ratio due to increase in the amount of bismuth vanadate. The crystallite size was calculated using Debye-Scherrer equation were found to be 41.7 nm for $BiVO_4$, 34.3 nm for (1:1) and 35.7 nm (2:1) ratio heterojunction.

$$D = \frac{K\lambda}{B(\cos\theta)} \quad (2)$$

where D is the mean size of crystallites (nm); K is a factor 0.9; λ is X-ray wavelength; B is FWHM; θ is the Bragg angle.

In case of the heterojunction the absorbance peak shifted towards the visible range which also supports the narrow band gap energy of 2.5 eV which observed in Tauc plot of Fig. 4 (B).

Morphological studies: The morphological analysis of the synthesized materials was performed using FESEM, as shown in Fig. 2. The pristine CoO particles exhibited a cubical, heterogeneous structure with some degree of agglomeration. In contrast, the FESEM image of $BiVO_4$ revealed predominantly uniform, monodispersed floral-shaped particles. The aggregated nanoparticles displayed a substantial amount of irregular, smaller crystals within the clusters [20]. In contrast, the heterojunction sample exhibits an irregular packing of particles of varying sizes, with a mosaic-like arrangement that forms aggregated block structures. This significant morphological difference from the reference $BiVO_4$ indicates that the introduction of cobalt plays a crucial role in modulating the morphology of $BiVO_4$. This effect likely arises from the preferential formation of CoO on the $BiVO_4$ surface, which influences the growth rates of each crystal face of $BiVO_4$, resulting in the observed structural variation. In EDX result, the addition of Co with O, Bi, V confirmed the successful formation of hetrojunction.

Optical studies: The optical property of the fabricated catalyst was studied using UV-DRS analysis and the results shown in Fig. 3a indicated the poor visible light absorbtion capacity of bismuth vanadate, which is a major obstacle for using it as a effective photocatalyst. In case of the heterojunction the absobance peak shifted towards the visble range, which also supports the narrow band gap energy of 2.5 eV, which observed in Tauc plot (Fig. 3b).

Photocatalytic activity: The photocatalytic efficiency of synthesized catalysts were tested by degradation of malachite green dye under solar light and for indepth study for the effect of factors on degradation different parameters like pH, concentration of dye solution, catalyst dose were varied as shown in Fig. 4. The point zero charge (pH_{pzc}), which plays a vital role in the degradation performance. The pH_{pzc} of bismuth vanadate and the heterojunction (1:1) and (2:1) were found to be 4.5, 6.7, 6.2, respectively. The charge of the catalyst surface remains

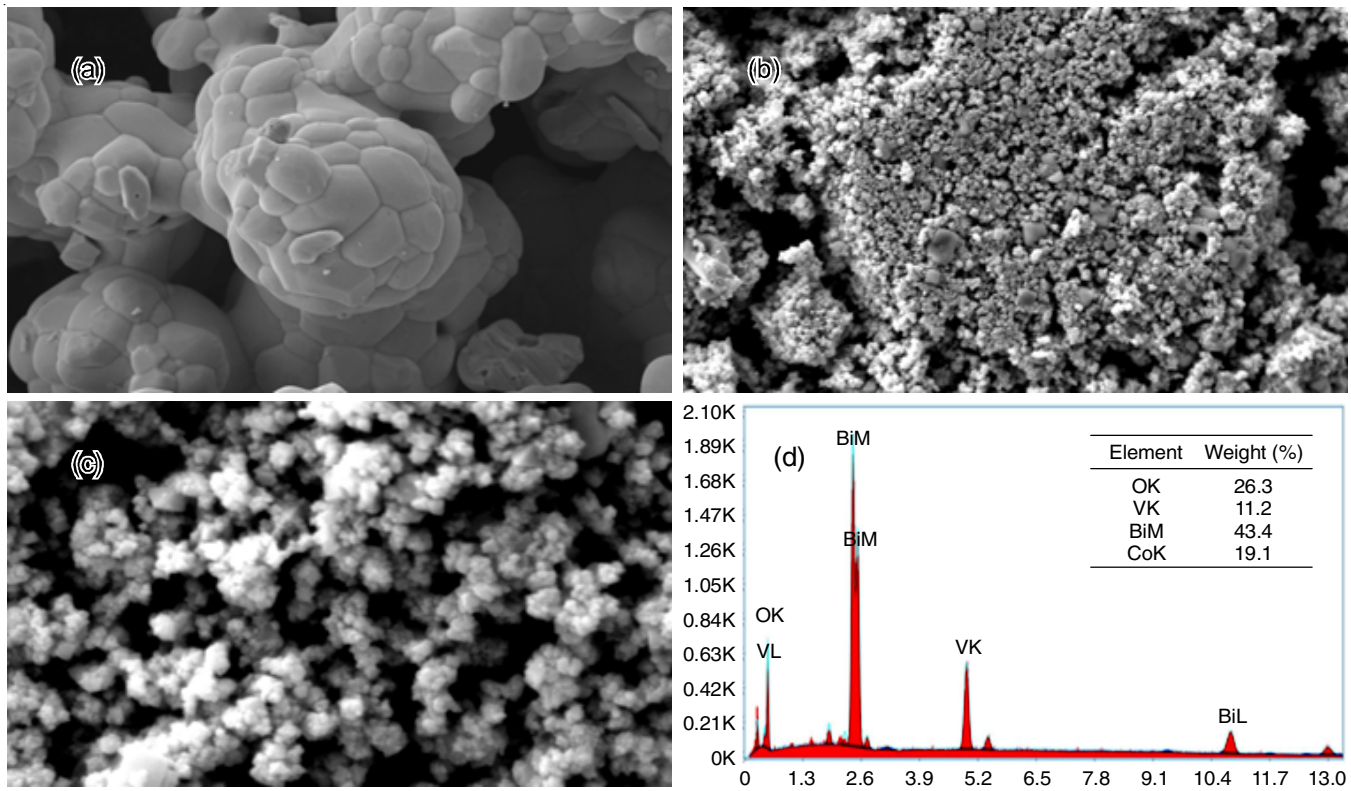

Fig. 2. FE-SEM images (a,b,c), EDX (d) of $BiVO_4$, CoO, $BiVO_4$/CoO (1:1)

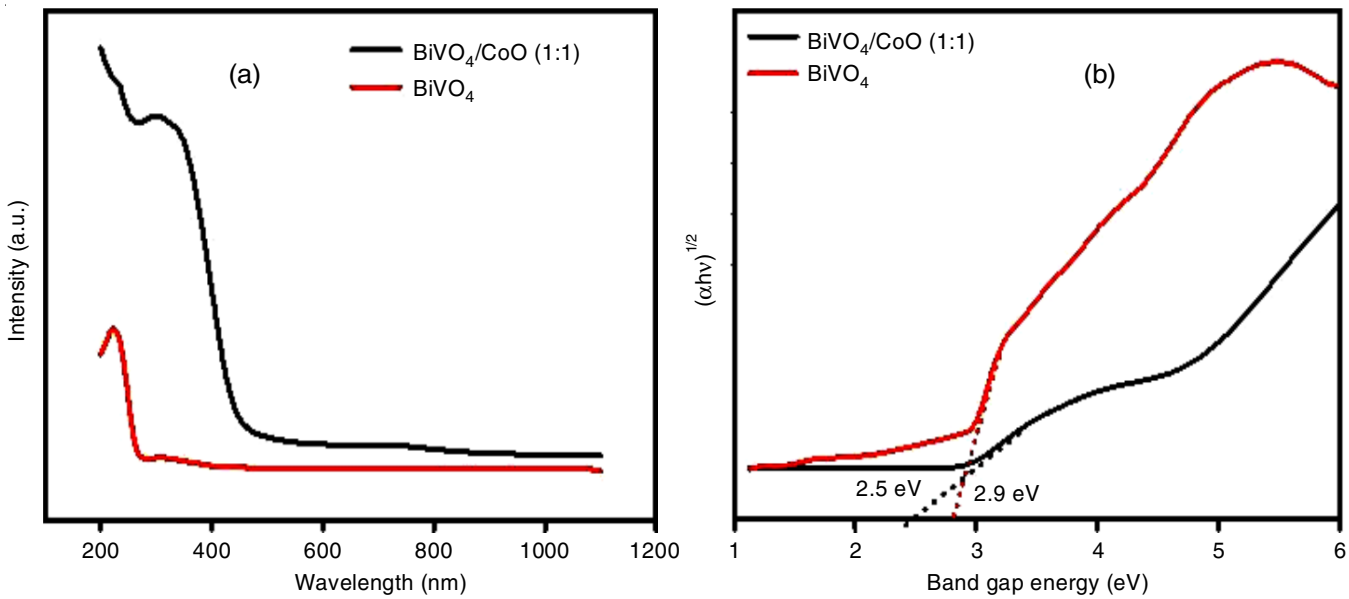

Fig. 3. UV-DRS spectra (a) and Tauc plot of $BiVO_4$, $BiVO_4$/CoO (1:1) (b)

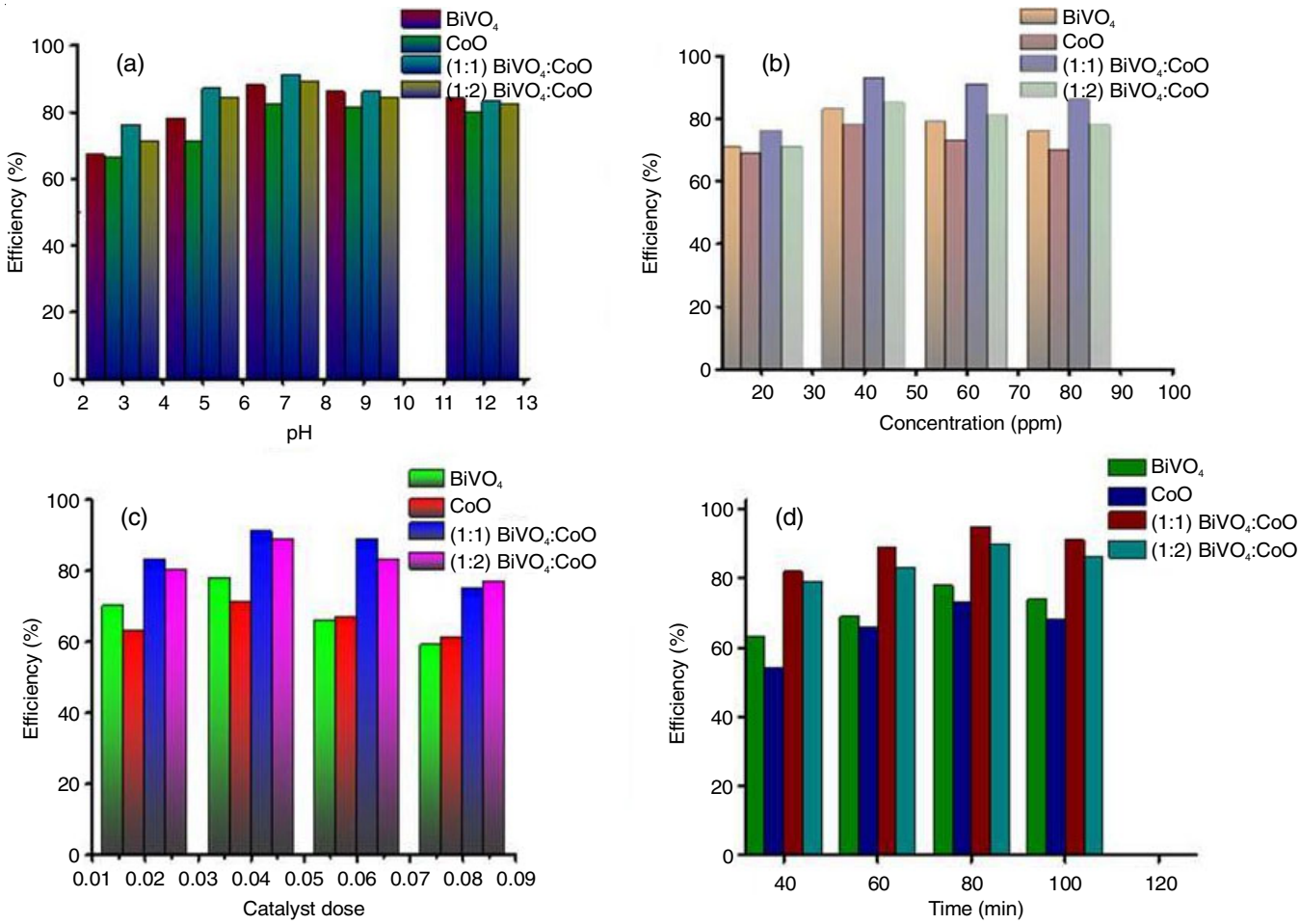

Fig. 4. Effects of pH (a), photocatalyst dose, (b) ([MG] = 100 ppm), Malachite green (MG) dye concentration (c), and time (d) on photocatalytic degradation under solar light

neutral below this value surface becomes positive charge and above this converts the surface negative charged. The pH *vs.* degradation result is shown in Fig. 4a, where the maximum degradation result of 83% was achieved by $BiVO_4$/CoO (1:1) at pH 7. To study the effect of dye concentration on degradation different concentrations (20, 40, 60, 80 ppm) were taken by keeping pH ~ 7 giving the best result. The results (Fig. 4b) show that as the concentration increases from 20 to 40 ppm, the degra-

dation percentage increased due to the increased interaction between the catalyst's active site and the dye molecule. After reaching 40 ppm with further increase in the concentration the degradation percentage slipped down slightly. This is because after an optimum concentration with rising further the solar light penentration gets disrupted due to the formation of layer on the water surface. The maximum degradation of 84% was achieved on 40 ppm malachite green dye solution. The effect of catalyst dose on the degradation percentage was studied by using 20, 40, 60, 80 mg catalyst on 50 mL of 40 ppm malachite green dye at pH ~ 7. The maximum degradation of 84% was achieved with 40 mg catalyst, which got reduced with increasing the dose due the overcrowding of catalysts and bombarding of catalysts with each other leads to deactivation of catalysts.

The kinetics of the synthesized catalyst for malachite green dye photodegradation were analyzed using the Langmuir–Hinshelwood model (eqn. 3):

$$kt = \ln\frac{C}{C_o} \quad (3)$$

where k is the rate constant, t is time, and C and C_0 are the initial and final concentrations.

As shown in Fig. 5e, the linear plots indicate pseudo-first-order kinetics with R^2 values of 0.9943 for $BiVO_4$, 0.9929 for CoO and 0.9971 for $BiVO_4$/CoO.

Mechanism: Reactive species including superoxide radical anions ($^{\bullet}O_2$), hydroxyl radicals ($^{\bullet}OH$) and photoinduced holes (h^+), play a key role in the photodegradation of pollutants. The effectiveness of these species in degrading pollutants follows the order: $^{\bullet}OH > {}^{\bullet}O_2^- > h^+$. The degradation rate of malachite green (MG) dropped significantly when scavengers for these radicals AO, BQ and BuOH were added, with the most substantial decrease observed in the presence of *t*-butyl alcohol (BuOH), indicating the dominant role of $^{\bullet}OH$ radicals. Superoxide radical anions ($^{\bullet}O_2^-$) also contribute to MG degradation, as shown by a reduction in activity when BQ was added. In contrast, the addition of AO caused only a minor reduction in MG photodegradation efficiency, suggesting that photo-induced holes (h^+) have a limited role in the degradation process shown in Fig. 5a [21].

Reusability studies: The reusability of the $BiVO_4$/CoO photocatalyst was tested over five cycles for the photodegradation of 25 ppm malachite green under visible light. The catalyst maintained high degradation efficiency, with around 78.1% malachite green dye removal after the third cycle. The slight decrease in efficiency in the third cycle, compared to the first, is likely due to the accumulation of intermediates during the photocatalytic process [22] (Fig. 5b). To study the effect of adsorption on this degradation the catalyst added dye solution was kept in stirring for the same time in dark place as under sun to achieve the adsorption-desorption equilibrium and in every 20 min interval the dye solution was taken for UV study. It is observed that the degradation due to adsorption is minimal which was around 14% (Fig. 5c). To assess the photocatalytic mineralization of malachite green dye, total organic carbon (TOC) was measured. Fig. 5d shows the TOC removal rate for malachite green dye using $BiVO_4$/CoO photocatalysts. The study found that the TOC removal rate of malachite green dye rise with irradiation time, reaching 80%, indicating full breakdown but leaving some carbon behind. The study found that nanocomposite improves malachite green dye degradation efficiency and mineralization ability. The equations governing the degradation mechanism are provided below:

$$\text{Catalyst} + h\nu \longrightarrow e^-(CB) + h^+(VB) \quad (3)$$

$$O_2 + e^-(CB) \longrightarrow O_2^{\bullet-} \quad (4)$$

$$h^+(VB) + H_2O \longrightarrow OH^{\bullet} + H^+ \quad (5)$$

$$(MG, MB) + O_2^{\bullet-} + OH^{\bullet} \longrightarrow H_2O \quad (6)$$

A strategy to enhance the photocatalytic performance of $BiVO_4$/CoO composites is proposed based on the experimental results shown in Fig. 6. The formation of a heterojunction between $BiVO_4$ and CoO boosts photocatalytic activity under visible light. In this process, photo-generated holes in the valence band (VB) of CoO transfer to $BiVO_4$, while electrons move from the conduction band (CB) of $BiVO_4$ to CoO. This electron transfer helps degrade organic pollutants into H_2O and CO_2 through reactions where electrons interact with H_2O and OH^- and holes react with O_2 to form O_2^- and $^{\bullet}OH$ radicals, facilitating the degradation. The $BiVO_4$/CoO catalysts clearly increased the photocatalytic activity in comparison to $BiVO_4$ and not only improved the utilization of visible light but also successfully suppressed the combination rate of electron-hole pairs. Unlike $BiVO_4$ alone, the $BiVO_4$/CoO catalysts effectively reduced the recombination rate of electron-hole pairs under visible light, while simultaneously increasing their utilization. This improvement led to a notable enhancement in the photocatalytic activity.

Comparative studies: A comparative study on the degradation efficiency of different $BiVO_4$ catalysts shown in Table-1 from which CoO/$BiVO_4$ nanocomposite has shown better photocatalytic activity as compared to others showing result under UV light.

TABLE-1
COMPARATIVE STUDY ON DEGRADATION EFFICIENCY OF $BiVO_4$ BASED PHOTOCATALYSTS

Catalyst	Dye	Degradation (%)	Time (min)	Ref.
Ag/La-$BiVO_4$	XyO	93.00	180	[23]
	RhB	95.00		
Fe-doped $BiVO_4$	Ibuprofen	80.00	180	[24]
RGO-$BiVO_4$	Ciprofloxacin	68.20	60	[25]
m-$BiVO_4$	RhB	64.81	120	[18]
	CV	96.23	210	
$BiVO_4$	MB	97.20	105	[26]
Ag-doped $BiVO_4$	MR	90.80	125	[27]
$BiVO_4$/CoO (1:1)	MG	84.00	80	This work

Conclusion

In summary, $BiVO_4$/CoO nanocomposites were successfully synthesized using a co-precipitation method with varying pH levels to degrade malachite green dye under sunlight. The nanocomposite (pH = 7) achieved nearly 84% degradation in 80 min, demon-strating excellent catalytic performance. CoO

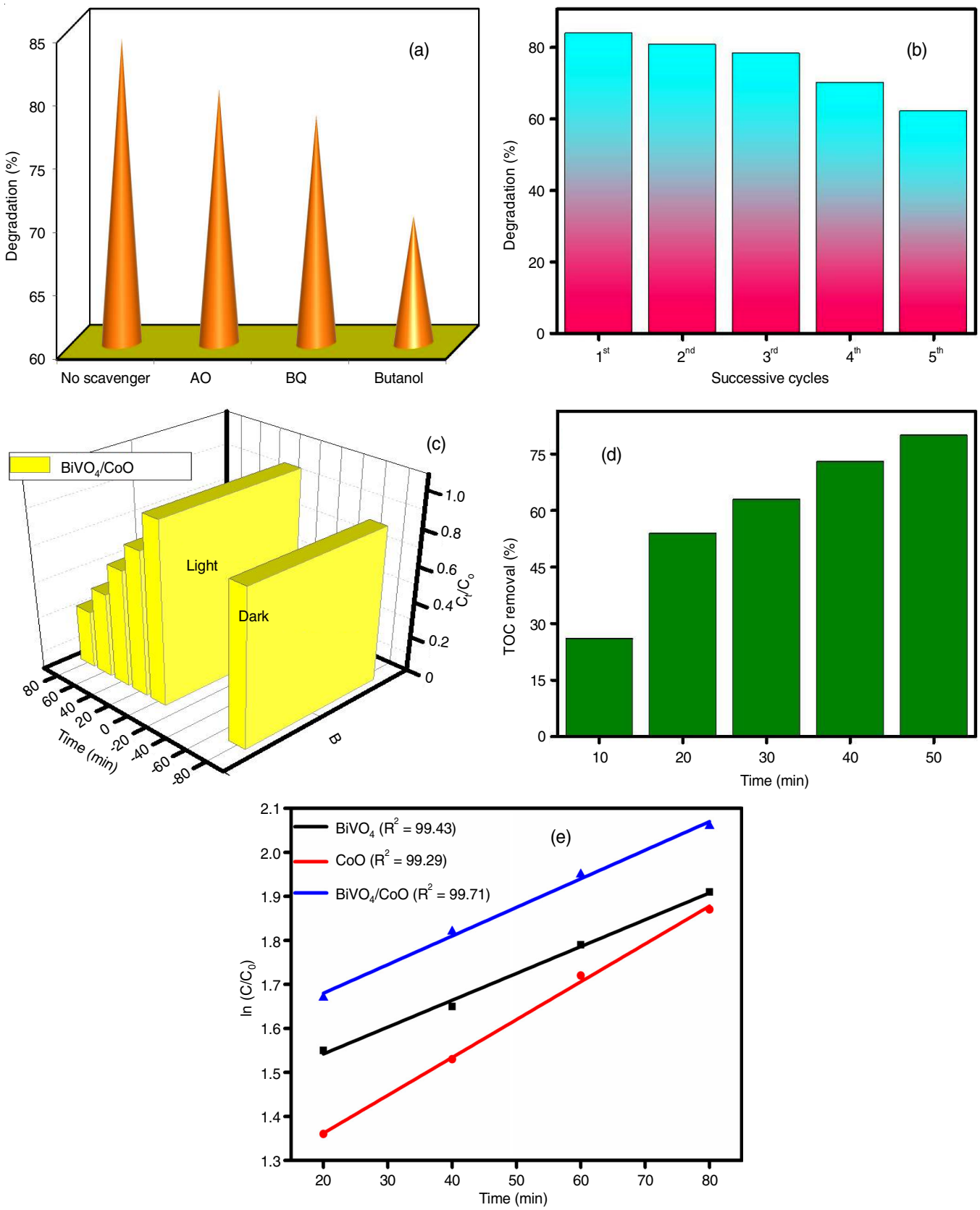

Fig. 5. Effects of pH (a), photocatalyst dose (b) ([MG] = 100 ppm), MG concentration (c), time (d) and (e) kinetic plot

doping enhanced visible light utilization and prevented electron-hole recombination. The pH of the synthesis process influenced the crystal structure and morphology of the catalyst, which in turn affected its photocatalytic efficiency. Adjusting the pH resulted in a nanocomposite with improved stability and photocatalytic performance.

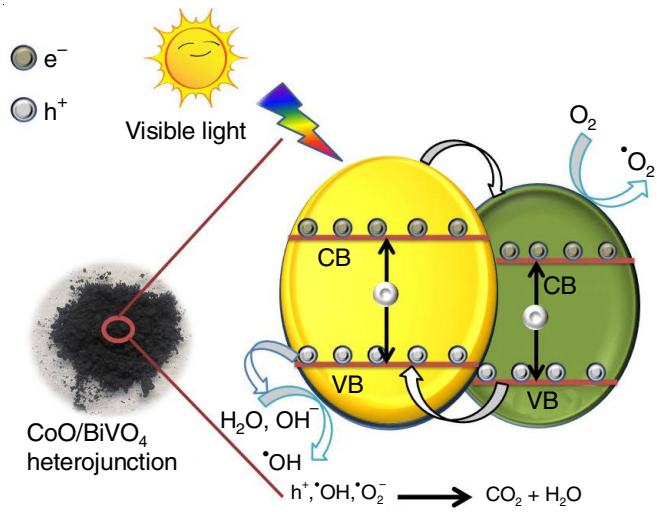

Fig. 6. Potential photocatalytic mechanism for $BiVO_4$/CoO catalysts for the breakdown of malachite green dye when exposed to visible light

CONFLICT OF INTEREST

The authors declare that there is no conflict of interests regarding the publication of this article.

REFERENCES

1. C. You, C. Wang, M. Cai, Y. Liu, B. Zhu and S. Li, *Acta Phys.-Chim. Sin.*, **40**, 2407014 (2024); https://doi.org/10.3866/PKU.WHXB202407014
2. S. Li, M. Cai, C. Wang and Y. Liu, *Adv. Fiber Mater.*, **5**, 994 (2023); https://doi.org/10.1007/s42765-022-00253-5
3. A. Chuenkruit, W. Thongjoon, K. Aiempanakit, M. Aiempanakit and C. Aiempanakit, *J. Metals Mater. Miner.*, **34**, 1964 (2024); https://doi.org/10.55713/jmmm.v34i4.1964
4. S. Rasheed, F. Sher, T. Rasheed, S. Sehar, M. Al Qubeissi, F. Zafar and E.C. Lima, *Mater. Chem. Phys.*, **270**, 124837 (2021); https://doi.org/10.1016/j.matchemphys.2021.124837
5. A. Malathi and J. Madhavan, *J. Nano Res.*, **48**, 49 (2017); https://doi.org/10.4028/www.scientific.net/JNanoR.48.49
6. F. Mohamadpour and A.M. Amani, *RSC Adv.*, **14**, 20609 (2024); https://doi.org/10.1039/D4RA03259D
7. W. Zamani, S. Rastgar and A. Hedayati, *Sci. Rep.*, **13**, 18182 (2023); https://doi.org/10.1038/s41598-023-45274-1
8. X. Wang, J. Song, J. Huang, J. Zhang, X. Wang, R.R. Ma, J. Wang and J. Zhao, *Appl. Surf. Sci.*, **390**, 190 (2016); https://doi.org/10.1016/j.apsusc.2016.08.040
9. Z. Qiao, T. Yan, W. Li and B. Huang, *New J. Chem.*, **41**, 3134 (2017); https://doi.org/10.1039/C6NJ04119A
10. C. Shen, X. Li, B. Xue, D. Feng, Y. Liu, F. Yang, M. Zhang and S. Li, *Appl. Surf. Sci.*, **679**, 161303 (2025); https://doi.org/10.1016/j.apsusc.2024.161303
11. M. Ashokkumar and P. Arunachalam, *Appl. Catal. A Gen.*, **555**, 47 (2018); https://doi.org/10.1016/j.apcata.2018.02.010
12. S. Sun and W. Wang, *RSC Adv.*, **4**, 47136 (2014); https://doi.org/10.1039/C4RA06419D
13. S. Balakumar, N. Mahesh, M. Kamaraj, S. Shyamalagowri, J. Manjunathan, S. Murugesan, J. Aravind and P.S. Babu, *Chemosphere*, **303**, 135052 (2022); https://doi.org/10.1016/j.chemosphere.2022.135052
14. B. Li, X.-J. Liu, H.-W. Zhu, H.-P. Guan and R.-T. Guo, *Small*, **20**, 2406074 (2024); https://doi.org/10.1002/smll.202406074
15. X. Liu, S. Gu, Y. Zhao, G. Zhou and W. Li, *J. Mater. Sci. Technol.*, **56**, 45 (2020); https://doi.org/10.1016/j.jmst.2020.04.023
16. A.A. Oladipo and F.S. Mustafa, *Beilstein J. Nanotechnol.*, **14**, 291 (2023); https://doi.org/10.3762/bjnano.14.26
17. K. Qin, Q. Zhao, H. Yu, X. Xia, J. Li, S. He, L. Wei and T. An, *Environ. Res.*, 199, 111360 (2021); https://doi.org/10.1016/j.envres.2021.111360
18. M.M. Sajid, N. Amin, N.A. Shad, S.B. khan, Y. Javed and Z. Zhang, *Mater. Sci. Eng. B*, **242**, 83 (2019); https://doi.org/10.1016/j.mseb.2019.03.012
19. M. Montazerozohori, A. Masoudiasl, S. Farokhiyani, S. Joohari and P. McArdle, *Ultrason. Sonochem.*, **38**, 134 (2017); https://doi.org/10.1016/j.ultsonch.2017.03.017
20. D. Pradhan, S.K. Biswal, R. Singhal, P.K. Panda and S.K. Dash, *Surf. Interfaces*, **52**, 104954 (2024); https://doi.org/10.1016/j.surfin.2024.104954
21. X. Chen, M. Zhang, H. Qin, J. Zhou, Q. Shen, K. Wang, W. Chen, M. Liu and N. Li, *Sep. Purif. Technol.*, **280**, 119751 (2022); https://doi.org/10.1016/j.seppur.2021.119751
22. T.B. Nguyen and R.-A. Doong, *RSC Adv.*, **6**, 103428 (2016); https://doi.org/10.1039/C6RA21002C
23. S. Prabhavathy and D. Arivuoli, *Inorg. Chem. Commun.*, **141**, 109483 (2022); https://doi.org/10.1016/j.inoche.2022.109483
24. C. Regmi, Y.K. Kshetri, T.-H. Kim, R.P. Pandey and S.W. Lee, *Mol. Catal.*, **432**, 220 (2017); https://doi.org/10.1016/j.mcat.2017.02.004
25. Y. Yan, S. Sun, Y. Song, X. Yan, W. Guan, X. Liu and W. Shi, *J. Hazard. Mater.*, **250-251**, 106 (2013); https://doi.org/10.1016/j.jhazmat.2013.01.051
26. V. Sivakumar, R. Suresh, K. Giribabu and V. Narayanan, *Cogent Chem.*, **1**, 1074647 (2015); https://doi.org/10.1080/23312009.2015.1074647
27. S. Kausar, R.M. Munir, T. Iqbal, S. Afsheen, M.S. Mansha, A.M. Elgorban and H.A. Al-Shwaiman, *J. Inorg. Organomet. Polym. Mater.*, **34**, 6071 (2024); https://doi.org/10.1007/s10904-024-03236-8